ChemPubSoc Europe

DOI: 10.1002/batt.202000010

BATTERIES & SUPERCAPS
Articles

Gassing Behavior of High-Entropy Oxide Anode and Oxyfluoride Cathode Probed Using Differential Electrochemical Mass Spectrometry

Ben Breitung,*[a, b] Qingsong Wang,[a] Alexander Schiele,[a] Đorđije Tripković,[a] Abhishek Sarkar,[a, c] Leonardo Velasco,[a] Di Wang,[a, b] Subramshu S. Bhattacharya,[d] Horst Hahn,[a, c, e] and Torsten Brezesinski*[a]

Multicomponent materials may exhibit favorable Li-storage properties because of entropy stabilization. While the first examples of high-entropy oxides and oxyfluorides show good cycling performance, they suffer from various problems. Here, we report on side reactions leading to gas evolution in Li-ion cells using rock-salt $(Co_{0.2}Cu_{0.2}Mg_{0.2}Ni_{0.2}Zn_{0.2})O$ (HEO) or $Li(Co_{0.2}Cu_{0.2}Mg_{0.2}Ni_{0.2}Zn_{0.2})OF$ (Li(HEO)F). Differential electrochemical mass spectrometry indicates that a robust solid-electrolyte interphase layer is formed on the HEO anode, even when using an additive-free electrolyte. For the Li(HEO)F cathode, the cumulative amount of gases is found by pressure measurements to depend strongly on the upper cutoff potential used during cycling. Cells charged to 5.0 V versus Li^+/Li show the evolution of O_2, H_2, CO_2, CO and POF_3, with the latter species being indirectly due to lattice O_2 release as confirmed by electron energy loss spectroscopy. This result attests to the negative effect that lattice instability at high potentials has on the gassing.

1. Introduction

Rechargeable lithium-ion batteries (LIBs) are the most widely used electrochemical energy storage devices. They combine stable capacity retention with good energy density and efficiency, making them first choice for a variety of applications, such as in electric vehicles.[1–7] Nevertheless, especially energy-demanding applications necessitate the development of new low-voltage anode and high-voltage cathode materials with improved specific capacities (where energy storage is based on some form of battery storage, such as insertion, conversion or alloying reactions).[8–13] However, despite the possibility of achieving high specific capacities, currently used materials often fall short of capacity retention over cycling.

Very recently, a new class of multicomponent electrode materials has been reported, which seems promising for the development of next-generation LIBs.[14–17] These materials exhibit tailorable properties and good cycling performance and belong to the so-called high-entropy oxides (HEOs). HEOs are a class of materials where a large number of different (incorporated) elements increases the configurational entropy, leading to entropy stabilization.[18–21] The concept of entropy stabilization was first applied to metallic alloy systems and later transferred to ionic and covalently-bonded structures.[22–26] For high-entropy materials, a single-phase crystal structure can be achieved when the Gibbs free energy is negative or, in other words, when the entropy term is greater than the enthalpy of mixing.[27] The configurational entropy is determined by the number of different elements on the same sublattice (configurational entropy, S_{config}) and can be calculated according to Equation S1. The stabilization of a single-phase structure made from various elements may lead to unprecedented materials properties. Note that some of the constituent elements are likely incorporated into an atypical lattice structure and there is a large number of possible interactions between them.

Rock-salt HEOs constitute a prominent class of HEOs. One such compound, comprising five different types of cations, is

[a] Dr. B. Breitung, Dr. Q. Wang, Dr. A. Schiele, Dr. Đ. Tripković, A. Sarkar, Dr. L. Velasco, Dr. D. Wang, Prof. H. Hahn, Dr. T. Brezesinski
Institute of Nanotechnology
Karlsruhe Institute of Technology (KIT)
Hermann-von-Helmholtz-Platz 1,
76344 Eggenstein-Leopoldshafen, Germany
E-mail: ben.breitung@kit.edu
torsten.brezesinski@kit.edu
[b] Dr. B. Breitung, Dr. D. Wang
Karlsruhe Nano Micro Facility
Karlsruhe Institute of Technology (KIT)
Hermann-von-Helmholtz-Platz 1,
76344 Eggenstein-Leopoldshafen, Germany
[c] A. Sarkar, Prof. H. Hahn
Joint Research Laboratory Nanomaterials
Technische Universität Darmstadt and Karlsruhe Institute of Technology (KIT)
Otto-Berndt-Str. 3,
64206 Darmstadt, Germany
[d] Prof. S. S. Bhattacharya
Department of Metallurgical and Materials Engineering
Nano Functional Materials Technology Centre
Indian Institute of Technology Madras
Chennai, 600036, India
[e] Prof. H. Hahn
Helmholtz Institute Ulm for Electrochemical Energy Storage
Helmholtzstr. 11, 89081 Ulm, Germany

Supporting information for this article is available on the WWW under https://doi.org/10.1002/batt.202000010

$(Co_{0.2}Cu_{0.2}Mg_{0.2}Ni_{0.2}Zn_{0.2})O$, which is referred to as HEO hereafter. As mentioned previously, because the stable crystal structure of some of the oxides of the constituent elements is not of rock-salt type (e.g., wurtzite ZnO or tenorite CuO), a certain enthalpy has to be overcome to allow formation of a single-phase material.[18] Recently, it has been shown that LIB cells using HEO as an anode active material are capable of delivering specific capacities of $\geq$600 mAh/g_{HEO} over hundreds of cycles.[14,28] Interestingly, extraction of a single cation species from the HEO led to not only a reduction in S_{config} (1.39 vs 1.61 R) but also a significant decline in cycling stability, with the latter being reminiscent of common conversion anode materials.[14] Furthermore, each individual element apparently exerts some specific effect on the Li-storage behavior (extraction of Cu led to a lower average lithiation potential while the respective compound without Zn revealed a two-step oxidation process, for example), thereby paving the way toward a modular approach to electrode materials with tailored properties.

In another study, it has been shown that S_{config} can be increased further by incorporation of different anions into the multicationic structure. In such HEOs, S_{config} is determined not only by the elements on the cation sublattice but also the different anion species. One such compound with S_{config} = 2.19 R, a high-entropy rock-salt oxyfluoride, $Li(Co_{0.2}Cu_{0.2}Mg_{0.2}Ni_{0.2}Zn_{0.2})OF$ (referred to as Li(HEO)F), was produced by mechanochemistry.[17] This particular material was found to exhibit promising electrochemical properties as a cathode active material for LIB applications.

In order to gain more insight into the reactions occurring in HEO- and Li(HEO)F-based LIB cells upon cycling, in the present work, we aimed at studying their gassing behavior using differential electrochemical mass spectrometry (DEMS) coupled with infrared (IR) spectroscopy and pressure measurements. We show by electrochemical measurements that cells using a HEO anode do not require the use of a fluoroethylene carbonate-containing electrolyte to achieve good capacity retention. This result is confirmed by DEMS, indirectly indicating the formation of a robust solid-electrolyte interphase (SEI), even when using a 'standard' electrolyte. For cells with a Li(HEO)F cathode, both DEMS and transmission electron microscopy (TEM) revealed the release of lattice oxygen with preservation of the parent rock-salt phase when charged to high potentials.

2. Results and Discussion

In this study, the gassing behavior of high-entropy anode and cathode materials, namely, $(Co_{0.2}Cu_{0.2}Mg_{0.2}Ni_{0.2}Zn_{0.2})O$ (HEO) and $Li(Co_{0.2}Cu_{0.2}Mg_{0.2}Ni_{0.2}Zn_{0.2})OF$ (Li(HEO)F), respectively, in coin-type LIB half-cells was investigated by DEMS and pressure measurements.[29,30] Both methods allow in situ monitoring of gas evolution during cycling. DEMS further allows identification of the respective gaseous species.

The HEO anode material was synthesized by the nebulized spray pyrolysis (NSP) method. High-resolution TEM (HRTEM, Figure 1a) and selected-area electron diffraction (SAED, Figure 1b) confirmed the high crystallinity and phase purity. The pattern in Figure 1b displays diffraction rings indicative of a polycrystalline rock-salt structure with space group *Fm*–3*m*. More details on the characterization are provided in Ref. [14], Ref. [15], Ref. [16].

In order to study the Li-storage properties of the HEO anode, battery cells were assembled using 1 M $LiPF_6$ in either ethylene carbonate:ethyl methyl carbonate (EC:EMC, LP57) or fluoroethylene carbonate:ethyl methyl carbonate (FEC:EMC) as electrolyte and cycled in constant current-constant voltage (CC-CV) mode in the voltage range between 10 mV and 2.5 V versus Li^+/Li, with 1/10th of the current being the termination criterion in the CV steps. In the first two activation or formation cycles, the C-rate was set to C/20. Thereafter, it was increased to C/5 for the subsequent cycles. A rate capability test with CC delithiation at different rates of C/2, C/5 and C/10 was also implemented in the cycling protocol (details given in Table S1).

Selected charge/discharge curves and the lithiation capacities achieved over the first 100 cycles are shown in Figure 2. The results are in good agreement with previously published data.[14] In recent years, it has been shown that the use of FEC instead of EC in LP57 electrolyte is beneficial to the long-term cycling performance of especially alloying and conversion anode materials. FEC is effective in stabilizing the SEI. This means the SEI layer that is formed during the cell formation is more robust and flexible compared to that achieved using EC-

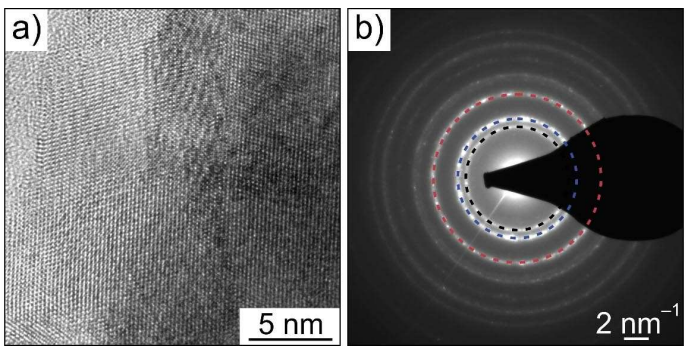

Figure 1. (a) HRTEM micrograph and (b) SAED pattern of the HEO anode material. The 111, 200 and 220 reflections of the rock-salt phase are denoted by dashed black, blue and red circles, respectively.

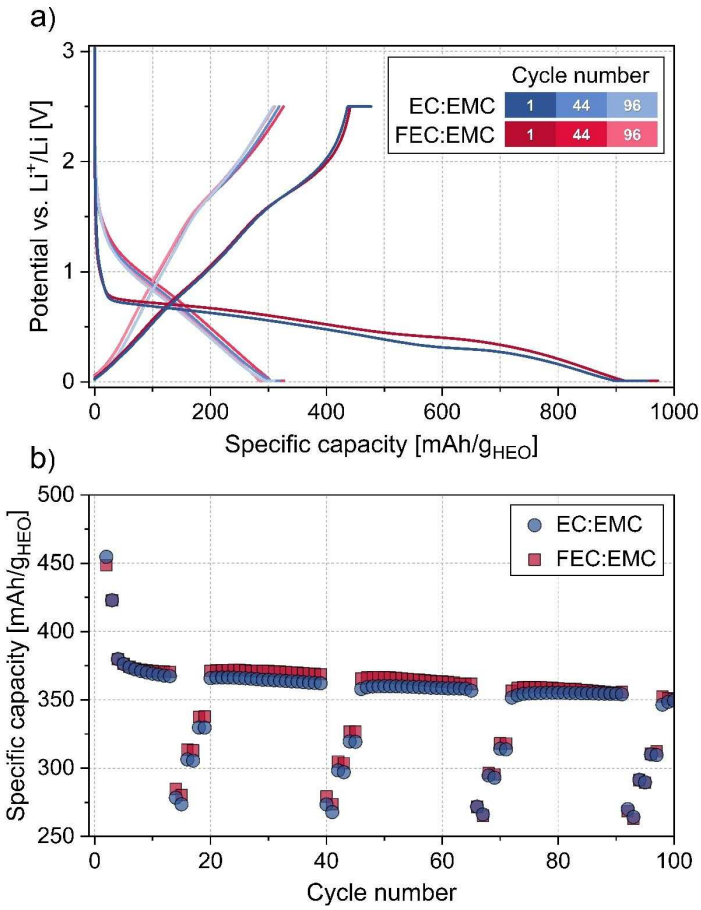

Figure 2. Cycling performance of the HEO anode material in a LIB half-cell at a C/5 rate in the voltage range of 10–2500 mV versus Li^+/Li. (a) Voltage profiles for the initial cycle at C/20 and for the 44th and 96th cycles at C/10 during rate performance testing. (b) Specific lithiation capacities over the first 100 cycles. LP57 (blue) or 1 M $LiPF_6$ in FEC:EMC (red) was used as electrolyte.

based electrolyte systems. Hence, it can better withstand volume changes upon Li insertion and extraction.[31–34] Also, the electrochemical decomposition of FEC occurs earlier in the charge process of full cells, that is, at relatively higher anode potentials. For both electrolyte systems, a specific capacity of >950 mAh/g_{HEO} was achieved in the initial cycle at C/20, followed by 370 mAh/g_{HEO} at C/5 from the 10th cycle onward. After 100 cycles, the cells were still capable of delivering 350 mAh/g_{HEO}, corresponding to an average capacity decline per cycle of 0.06% (between the 10th and 100th cycles). The long-term cycling performance is presented in Figure S1, showing specific lithiation capacities of 330 and 315 mAh/g_{HEO} for the FEC- and EC-based cells, respectively, after 600 cycles. This means the overall rate of capacity decline per cycle was <0.03%. As mentioned above, rate capability tests without CV step at the upper cutoff potential were implemented every 26 cycles. In the initial test after 14 cycles, specific capacities of 275–285, 305–315 and 330–340 mAh/g_{HEO} at rates of C/2, C/5 and C/10, respectively, were achieved for both electrolyte systems, with the FEC-based cells delivering slightly higher capacities. In the 22nd test after 586 cycles, the specific capacities were lower by up to 60 mAh/g_{HEO}. Taken together, the data shown in Figures 2 and S1 demonstrate that, irrespective of the electrolyte used, the HEO anode can be cycled stably for hundreds of cycles. Nevertheless, in order for HEO to have any practical relevance, several showstoppers, such as the poor first-cycle efficiency and the large voltage hysteresis, must be addressed, which is beyond the scope of the current paper.

In order to learn more about the stability of the SEI and the side reactions occurring with cycling, the gas evolution was studied in situ using DEMS. To this end, again, LIB half-cells with LP57 electrolyte were assembled and cycled at a C/10 rate in the same voltage range of 10–2500 mV versus Li^+/Li for three cycles. The correlation of the voltage profile with the evolved gases is shown in Figure 3. The most prominent gaseous species were found to be H_2 ($m/z=2$) and C_2H_4 ($m/z=26$). The latter mass fragment was used to determine the ethylene evolution since $m/z=28$ may be affected by fragments of CO_2, CO and N_2. The largest peak of H_2 evolution was observed at the beginning of cycling when the cell potential decreased rapidly from ~3.0 V to below 800 mV within less than 1 h. The main contribution to H_2 formation was probably the reduction of trace H_2O stemming from the cell parts, the separator, the electrode and/or the electrolyte. Additional H_2 evolution was apparent near the lower cutoff potential. Similar

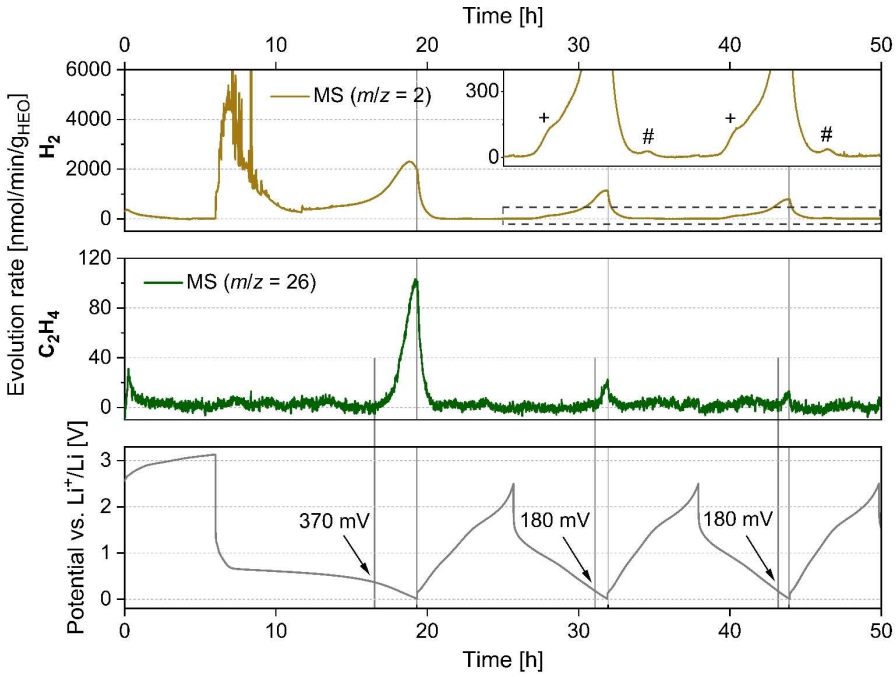

Figure 3. Gassing behavior of the HEO anode material in a LIB half-cell using LP57 electrolyte at a C/10 rate in the voltage range of 10–2500 mV versus Li^+/Li. Voltage profiles (gray) for the first three cycles and the corresponding gas evolution of H_2 ($m/z = 2$, gold) and C_2H_4 ($m/z = 26$, green) are shown. The inset in the upper panel is a 'zoomed-in' view of the area denoted by the dashed rectangle.

to the initial cycle, the highest H_2 evolution rate was observed at the lower cutoff potential in the 2nd and 3rd cycles. In addition, the presence of relatively weak (shoulder) peaks was noticed at ~850 mV and 1.3 V during lithiation and delithiation, respectively (denoted by symbols in the upper panel in Figure 3). These local maxima in the H_2 evolution curve may be indicative of the same reaction(s), with the difference in potential being due to overpotential.

The formation of H_2 was found to be accompanied by C_2H_4 evolution, starting at ~370 mV and also reaching the highest rate at the lower cutoff potential. C_2H_4 evolution is characteristic of the reductive decomposition of EC during SEI formation on graphite anodes and has been also detected for silicon anodes.[34–36] We assume that similar potential-dependent reactions occur on the free surface of the HEO electrode. In the 2nd and 3rd cycles, the amount of evolved C_2H_4 decreased significantly and the onset potential was shifted to lower values (~180 mV). This result suggests the formation of a fairly stable SEI and helps to explain the good cycling stability of the FEC-free HEO-based cells (see Figures 2 and S1).

The Li(HEO)F cathode material was prepared by mechanochemistry using HEO and LiF as precursors. During the milling process, both the Li^+ and F^- ions are incorporated into the rock-salt lattice, producing an insertion cathode material with a working potential of ~3.4 V versus Li^+/Li.[17] The cyclability of a Li(HEO)F-based LIB half-cell with LP57 electrolyte at a C/8 rate in the voltage range between 2.0 and 4.6 V versus Li^+/Li is shown in Figure 4. The initial specific discharge or lithiation capacity was 117 mAh/$g_{Li(HEO)F}$ and decreased in a rather linear fashion to 86 mAh/$g_{Li(HEO)F}$ during the first 30 cycles. However, thereafter, the specific capacity starts to increase again, as shown recently.[17] Similar to the HEO anode, the first-cycle Coulombic efficiency was relatively low but stabilized above 95% after the 5th cycle. The capacity loss with cycling and the irreversibilities are believed to be partially because of electrolyte degradation (oxidation) and cathode SEI (cSEI) formation. We note again that the oxide and oxyfluoride compounds employed in this work belong to a relatively new class of electrode materials and have not yet been optimized for LIB applications. Nevertheless, the preliminary data, especially for the new cathode active material, are promising.

In order to examine the side reactions leading to gas evolution, DEMS measurements were conducted on LIB half-cells with Li(HEO)F and LP57 as cathode and electrolyte, respectively. The cells were charged at a C/10 rate to different upper cutoff potentials of 4.6, 4.8 and 5.0 V for three cycles while keeping the lower cutoff potential at 2.0 V versus Li^+/Li. The 5.0 V results are shown in Figure 5 (see Figures S2 and S3 for the 4.8 and 4.6 V DEMS data, respectively). During the measurement, several different gaseous species were detected, all showing similar evolution patterns, with the highest evolution rates being for H_2 ($m/z = 2$) and CO_2 ($m/z = 44$). The onset potential of CO_2 evolution in the initial cycle was ~4.55 V, while H_2 shared a slightly higher onset potential of 4.75 V with CO (detected via IR absorption) and POF_3 ($m/z = 85$ and 104). The highest evolution rates for all mentioned species were detected at the upper cutoff potential and they decreased rapidly when switching to the discharge cycle. A slightly different evolution profile was observed for O_2 in the initial cycle. While the onset potential of O_2 was similar to that of CO_2 (4.55 V), the evolution peak reached its maximum at 4.65 V, with a decreasing rate afterwards until 4.75 V where no further

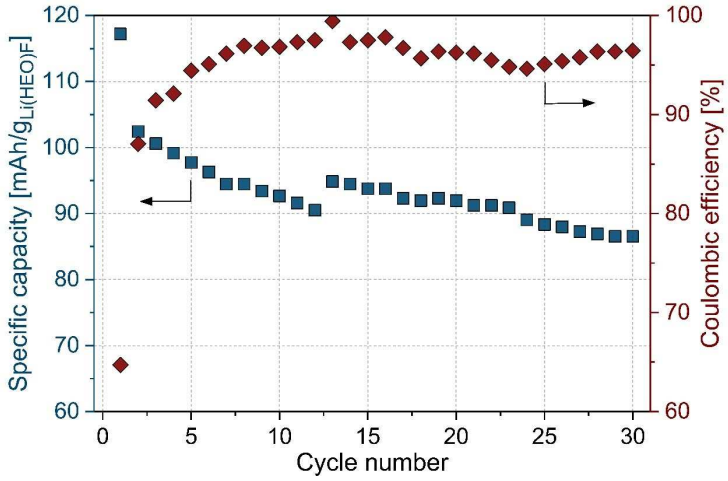

Figure 4. Cycling performance of the Li(HEO)F cathode material in a LIB half-cell using LP57 electrolyte at a C/8 rate in the voltage range of 2.0–4.6 V versus Li^+/Li. Specific lithiation capacities and Coulombic efficiencies over the first 30 cycles are shown.

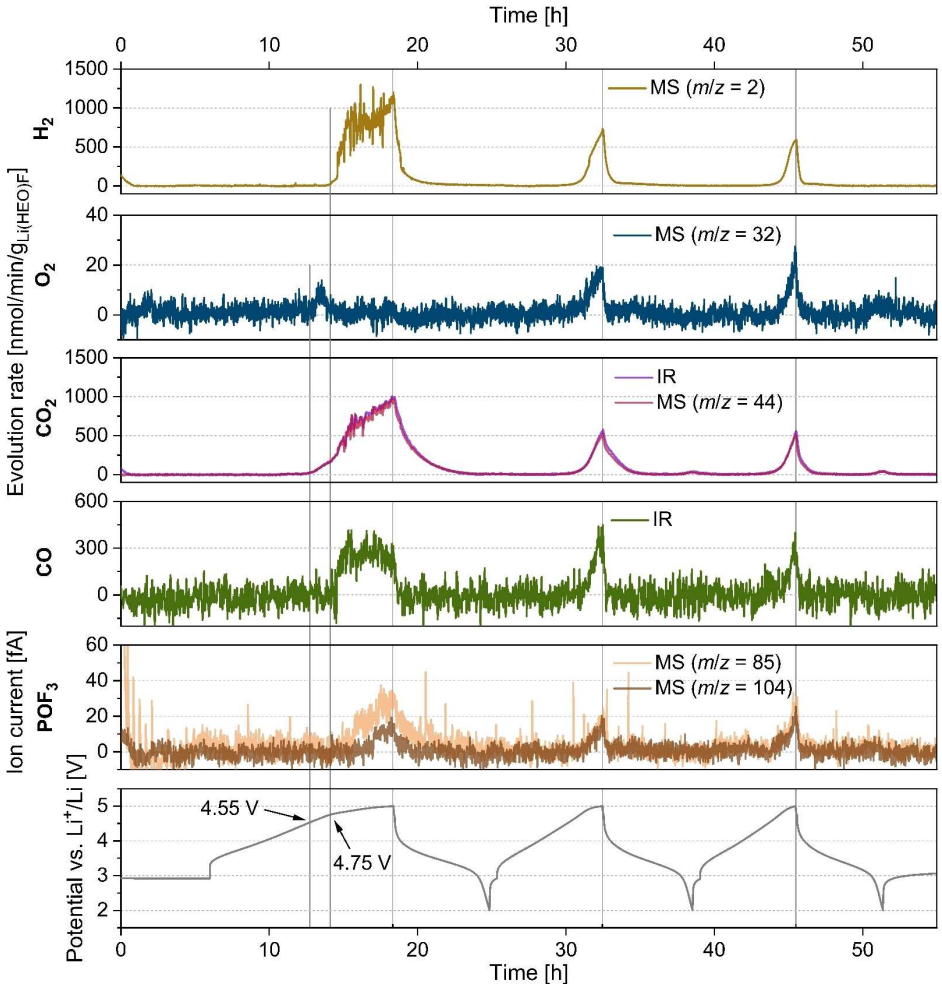

Figure 5. Gassing behavior of the Li(HEO)F cathode material in a LIB half-cell using LP57 electrolyte at a C/10 rate in the voltage range of 2.0–5.0 V versus Li^+/Li. Voltage profiles (gray) for the first three cycles and the corresponding gas evolution of H_2 ($m/z = 2$, gold), O_2 ($m/z = 32$, blue), CO_2 ($m/z = 44$, pink; and via IR spectroscopy, purple), CO (via IR spectroscopy, green) and POF_3 ($m/z = 85$, orange; and $m/z = 104$, brown) are shown.

O_2 release could be detected. The same unexpected behavior was found for the cell with the cutoff potential of 4.8 V (Figure S2) but remarkably not for the cell charged to 4.6 V, for which no H_2 or CO evolution was detected (Figure S3). During

the 2nd and 3rd cycles, all evolved gaseous species exhibited virtually the same evolution profiles with onset potentials of ~4.75 V and maximum evolution rates at the upper cutoff potential. This result leads us to the conclusion that the processes causing the gassing are connected, although the previously mentioned characteristics of O_2 evolution during the initial cycle do not fit the concept. One possible scenario is the following: (i) Oxygen ions in the rock-salt lattice start to get oxidized at potentials around 4.75 V and are then released as reactive singlet oxygen. This behavior has been reported for layered Ni-rich $LiNi_xCo_yMn_zO_2$ (NCM) cathode active materials, for example. In the latter case, oxygen release is accompanied by surface reconstruction from layered to rock-salt-like structure because of the intrinsic instability of NCMs at high states of charge (SOC).[37–40] Because Li(HEO)F already exhibits a rock-salt structure, further investigations are required to elucidate the mechanism behind the oxygen evolution; however, it will be discussed in some more detail below. (ii) The release of reactive singlet oxygen and the high oxidative potential of the Li(HEO)F cathode lead to chemical and/or electrochemical decomposition of the carbonate-based electrolyte, resulting in the generation of CO_2 and CO (note that the active material is nanocrystalline in nature with a Brunauer-Emmett-Teller surface area of ~30 $m^2/g_{Li(HEO)F}$). (iii) Simultaneously with CO and CO_2 evolution, soluble decomposition products are formed, bearing protic groups, such as alcohols, and diffuse to the counter-electrode where they get reduced to produce H_2. (iv) In addition to H_2 formation, R-OH groups contribute to the decomposition of the conducting salt ($LiPF_6$).[41,42] According to Campion et al., $LiPF_6$ is prone to dissociation into LiF and PF_5, whereof the latter can react to POF_3, which was clearly detected in the DEMS measurement.[43]

The upper cutoff potential has a profound effect on the total amount of gas evolution. This is apparent in Figure 6 where integrated amounts of gases detected by DEMS are shown for the three different upper cutoff potentials (4.6, 4.8 and 5.0 V versus Li^+/Li). Additionally, a parallel set of experiments was conducted on the same type of cells by mounting a pressure sensor to measure the internal pressure changes because of gas evolution during cycling. In total, 12 individual cells were tested (4 cells per each upper cutoff potential). The results shown in Figure 6 follow the same trend as the DEMS data. The higher the cutoff potential, the larger is the increase in internal pressure. Furthermore, considering the experimental parameters ($\vartheta = 25\,^{\circ}C$, $V_{cell} \approx 5$ mL, $m_{Li(HEO)F} \approx 10$ mg),[30] the pressure increase of tens of mbar roughly corresponds to gas evolution in hundreds of micromoles per gram of active material, demonstrating also a reasonable quantitative agreement (Figure S4).

In order to better understand the redox reactions associated with the oxygen evolution, TEM and electron energy loss spectroscopy (EELS) measurements were performed. Because the oxygen release occurs at the interface between the electrolyte or SEI layer and the active material, the Li(HEO)F particles were probed for structural and oxidative changes after cycling at a C/10 rate in the voltage range of 2.0–5.0 V versus Li^+/Li. An indirect indication of oxygen loss at the top surface was derived from the near-edge structure of the O–K edge using EELS. Scanning TEM (STEM)/EELS line scans across cycled particles revealed distinct differences in the O–K edge between regions near the surface and close to the core. Specifically, the EEL spectra obtained from the edge (denoted by a blue square) and the center of the particle (denoted by a red rectangle) were integrated and compared to one another (Figure 7a). From Figure 7b, it is evident that the O–K edge of the bulk shows a much more prominent pre-peak at ~530 eV. The O–K edge is known to reflect the valence state of the constituent transition metals, with the pre-edge feature arising from the hybridization of the oxygen 2p and transition metal 3d states.[44,45] Here, the lower intensity of the pre-edge feature indicates the presence of more electrons occupying the 3d orbitals of the transition metals. This, in turn, suggests that the Li(HEO)F surface is in a less oxidized state (because of O_2 evolution). Hence, this result can be considered as an evidence of oxygen deficiency caused by O_2 evolution at high potentials. HRTEM of single particles of the same electrode demonstrated that the parent rock-salt phase is preserved, despite the lattice oxygen loss (Figure 7c). In addition, the overview micrograph in Figure 7d shows that most particles are still in a crystalline state and their size remains in the range between 10 and 20 nm, while the corresponding fast Fourier transform (FFT) pattern (Figure 7e) indicates the rock-salt-type structure.

3. Conclusions

In this work, we have confirmed the good capacity retention of HEO-based LIB half-cells, delivering specific capacities of >310 mAh/g_{HEO} after 600 cycles. Similar cycling performance and stability were found for cells using EC- and FEC-containing electrolytes. In situ gas analysis revealed that H_2 and C_2H_4 are the most prominent gaseous species upon cycling. After the initial cycle, especially the evolution rate of C_2H_4 decreased significantly, thereby indicating the formation of a robust SEI layer on the HEO particles and further emphasizing the unique entropy-stabilized (conversion-type) Li-storage mechanism.

Gas evolution in Li(HEO)F-based LIB half-cells was found both by DEMS coupled with IR spectroscopy and by pressure measurements to strongly depend on the upper cutoff potential used during cycling. Most of the gas evolution upon charging to 5.0 V versus Li^+/Li consisted of H_2 and CO_2 as well as smaller amounts of O_2, CO and POF_3. The formation of CO_2 and CO can be attributed to oxidative electrolyte decomposition at high potentials accompanied by the generation of protic species, triggering H_2 and POF_3 evolution. O_2 evolution is ascribed to lattice oxygen release from the surface layer of the Li(HEO)F particles, which was confirmed by EELS of the O–K edge. Interestingly, oxygen loss did not lead to notable changes in the parent rock-salt structure.

Taken together, the charge storage mechanism appears to be similar to that of Li-rich disordered rock-salt oxides and related compounds, with the relatively poor first-cycle efficiency and the gassing associated with the (singlet) O_2 evolution being major showstoppers. Nevertheless, in the

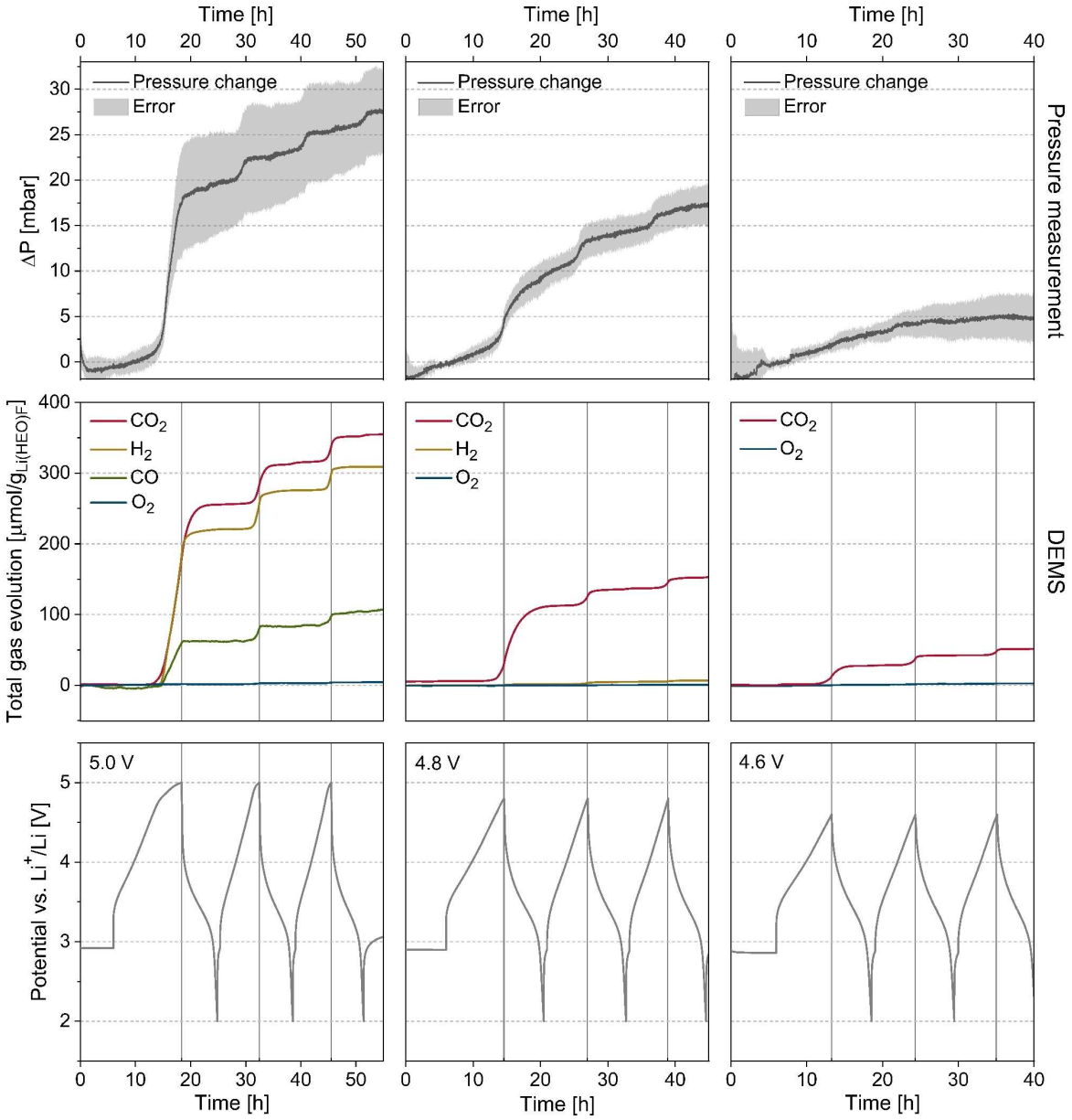

Figure 6. Effect of upper cutoff potential on the total amount of gas evolution during DEMS measurements on the Li(HEO)F-based LIB half-cells using LP57 electrolyte. The same trends are observed by measuring the increase in internal pressure.

future, high-entropy electrode materials might become viable alternatives for application in Li-ion batteries if their properties can be tailored in a favorable manner by compositional design, for example.

Experimental Section

Synthesis

HEO was prepared by the NSP method.[19] $Mg(NO_3)_2 \cdot 6H_2O$ (Sigma Aldrich, 99.9%), $Zn(NO_3)_2 \cdot 6H_2O$ (Alfa Aesar, 99.9%), $Cu(NO_3)_2 \cdot 2.5H_2O$ (Sigma Aldrich, 99.9%), $Ni(NO_3)_2 \cdot 6H_2O$ (Sigma Aldrich, 99.9%) and $Co(NO_3)_2 \cdot 6H_2O$ (Sigma Aldrich, 99.9%) served as precursors in the synthesis, with the final material forming in the gas phase of a hot-wall reactor at 1150 °C and subsequent sintering at 1000 °C for 1 h.[14–16]

Li(HEO)F was prepared by high-energy planetary ball-milling of a 1:1 molar mixture of LiF (Alfa Aesar, 99.99%) and HEO at 500 rpm for 24 h under an Ar atmosphere.[17] To this end, 50 ml WC vials and WC balls of 4 mm diameter were used, with the ball-to-powder ratio being 40:1 by weight.

Electrode Preparation

The HEO anode was prepared by casting a water-based slurry containing 63 wt% active material, 22 wt% Super C65 carbon black (Timcal) and 15 wt% Selvol 425 poly(vinyl alcohol) binder (Sekisui) onto Cu foil. The Li(HEO)F cathode was prepared by casting an N-methyl-2-pyrrolidone-based slurry containing 70 wt% active material, 20 wt% Super C65 carbon black and 10 wt% Solef 5130

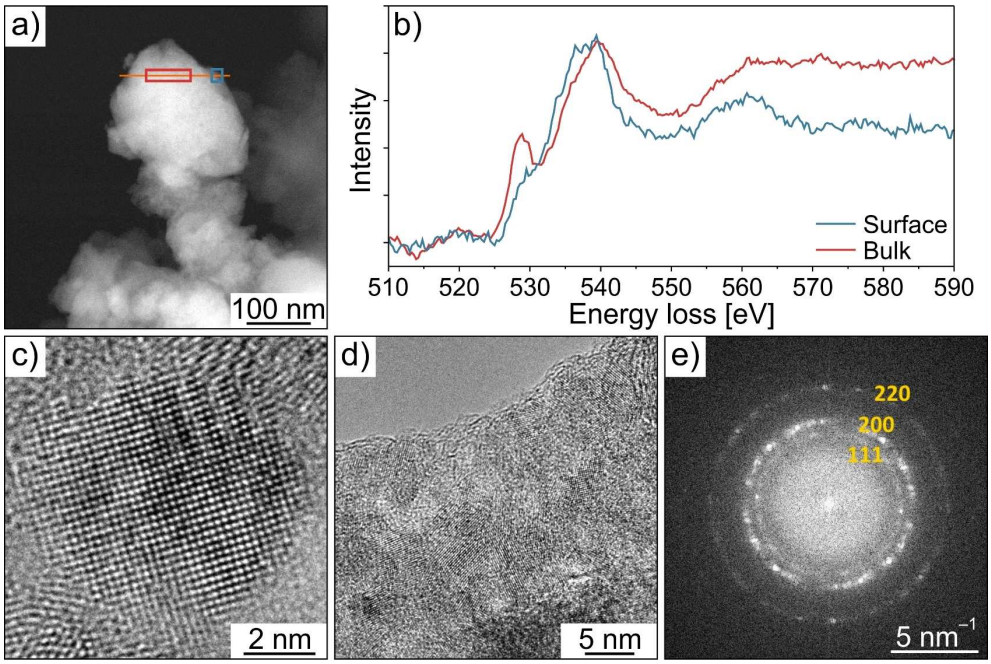

Figure 7. Electron microscopy of the Li(HEO)F cathode material after two cycles at a C/10 rate in the voltage range of 2.0–5.0 V. (a) STEM/EELS line scan and (b) O–K edge spectra for the areas denoted by the red (particle interior) and blue boxes (particle edge). (c) HRTEM micrograph of a single particle along the [100] zone-axis of the rock-salt structure. (d) Overview HRTEM micrograph and (e) corresponding FFT pattern.

polyvinylidene difluoride binder (Solvay) onto Al foil. The resultant electrodes were dried at 120 °C for 12 h in a vacuum. The active material loading was ~2.5 and 1.4 mg/cm^2 for the HEO anode and Li(HEO)F cathode, respectively.

Coin-type LIB cells were assembled in an Ar-filled glovebox (MBraun) with [O_2] and [H_2O] < 0.5 ppm by stacking 600 µm-thick Li counter-electrode (Albemarle Germany GmbH), Whatman GF/A or GF/D film separator (GE Healthcare Life Sciences) soaked with electrolyte solution and HEO or Li(HEO)F working electrode. For the HEO anode, two different electrolytes were used in the electrochemical testing, namely, 1 M $LiPF_6$ in either a 1:1 weight mixture of FEC (Solvay) and EMC (BASF SE) or a 3:7 weight mixture of EC (BASF SE) and EMC. The latter electrolyte is referred to as LP57.

Instrumentation

Galvanostatic charge/discharge measurements in CC–CV and CC modes were performed at 25 °C and at different C-rates (1 C = 1000 mA/g_{HEO} or 160 mA/$g_{Li(HEO)F}$) in the voltage range between 10 mV and 2.5 V and 2.0 V and 5.0, 4.8 or 4.6 V versus Li^+/Li for the HEO anode and Li(HEO)F cathode, respectively, using a MACCOR Series 4000 battery tester (Tulsa).

For DEMS and pressure measurements, a BioLogic VSP-300 potentiostat was used. Details about the setups can be found elsewhere.[29,30]

TEM was conducted on powder material dispersed on a holey carbon-coated gold grid. The samples were loaded onto a Gatan vacuum transfer holder inside a glovebox and transferred to the TEM without exposure to laboratory air. They were examined using a Titan 80–300 electron microscope (FEI) equipped with a CEOS image spherical aberration corrector, HAADF-STEM detector (Fischione model 3000) and Tridiem Gatan image filter (GIF). The microscope was operated at an accelerating voltage of 300 kV.

Conflict of Interest

The authors declare no conflict of interest.

Acknowledgements

Q.W. and B.B. acknowledge financial support by EnABLES. This project has received funding from the European Union's Horizon 2020 research and innovation program under grant agreement no. 730957. H.H. and Ab.S. acknowledge financial support from the Deutsche Forschungsgemeinschaft (DFG, grant no. HA 1344/43-1).

Keywords: lithium-ion battery · rock-salt structure · entropy stabilization · interfacial reactivity · oxygen evolution

[1] N. Nitta, F. Wu, J. T. Lee, G. Yushin, *Mater. Today* **2015**, *18*, 252–264.
[2] T. Kim, W. Song, D. Y. Son, L. K. Ono, Y. Qi, *J. Mater. Chem. A* **2019**, *7*, 2942–2964.
[3] G. Zubi, R. Dufo-López, M. Carvalho, G. Pasaoglu, *Renewable Sustainable Energy Rev.* **2018**, *89*, 292–308.
[4] J. Dąbrowa, M. Stygar, A. Mikuła, A. Knapik, K. Mroczka, W. Tejchman, M. Danielewski, M. Martin, *Mater. Lett.* **2018**, *216*, 32–36.
[5] A. Fotouhi, D. J. Auger, K. Propp, S. Longo, M. Wild, *Renewable Sustainable Energy Rev.* **2016**, *56*, 1008–1021.
[6] J. B. Goodenough, K.-S. Park, *J. Am. Chem. Soc.* **2013**, *135*, 1167–1176.
[7] V. Etacheri, R. Marom, R. Elazari, G. Salitra, D. Aurbach, *Energy Environ. Sci.* **2011**, *4*, 3243–3262.
[8] R. Marom, S. F. Amalraj, N. Leifer, D. Jacob, D. Aurbach, *J. Mater. Chem.* **2011**, *21*, 9938–9954.
[9] M. Yang, X. Zhao, Y. Bian, L. Ma, Y. Ding, X. Shen, *J. Mater. Chem.* **2012**, *22*, 6200–6205.

[10] R. Wang, X. Li, L. Liu, J. Lee, D.-H. Seo, S.-H. Bo, A. Urban, G. Ceder, *Electrochem. Commun.* **2015**, *60*, 70–73.
[11] Z. Lun, B. Ouyang, D. A. Kitchaev, R. J. Clément, J. K. Papp, M. Balasubramanian, Y. Tian, T. Lei, T. Shi, B. D. McCloskey, J. Lee, G. Ceder, *Adv. Energy Mater.* **2019**, *9*, 1802959.
[12] I. Mohammad, R. Witter, M. Fichtner, M. Anji Reddy, *Appl. Energy* **2018**, *1*, 4766–4775.
[13] M. A. Nowroozi, O. Clemens, *Appl. Energy* **2018**, *1*, 6626–6637.
[14] A. Sarkar, L. Velasco, D. Wang, Q. Wang, G. Talasila, L. de Biasi, C. Kübel, T. Brezesinski, S. S. Bhattacharya, H. Hahn, B. Breitung, *Nat. Commun.* **2018**, *9*, 3400.
[15] A. Sarkar, Q. Wang, A. Schiele, M. R. Chellali, S. S. Bhattacharya, D. Wang, T. Brezesinski, H. Hahn, L. Velasco, B. Breitung, *Adv. Mater.* **2019**, *31*, 1806236.
[16] Q. Wang, A. Sarkar, Z. Li, Y. Lu, L. Velasco, S. S. Bhattacharya, T. Brezesinski, H. Hahn, B. Breitung, *Electrochem. Commun.* **2019**, *100*, 121–125.
[17] Q. Wang, A. Sarkar, D. Wang, L. Velasco, R. Azmi, S. S. Bhattacharya, T. Bergfeldt, A. Düvel, P. Heitjans, T. Brezesinski, H. Hahn, B. Breitung, *Energy Environ. Sci.* **2019**, *12*, 2433–2442.
[18] C. M. Rost, E. Sachet, T. Borman, A. Moballegh, E. C. Dickey, D. Hou, J. L. Jones, S. Curtarolo, J.-P. Maria, *Nat. Commun.* **2015**, *6*, 8485.
[19] A. Sarkar, R. Djenadic, N. J. Usharani, K. P. Sanghvi, V. S. K. Chakravadhanula, A. S. Gandhi, H. Hahn, S. S. Bhattacharya, *J. Eur. Ceram. Soc.* **2017**, *37*, 747–754.
[20] R. Djenadic, A. Sarkar, O. Clemens, C. Loho, M. Botros, V. S. K. Chakravadhanula, C. Kübel, S. S. Bhattacharya, A. S. Gandhi, H. Hahn, *Mater. Res. Lett.* **2017**, *5*, 102–109.
[21] A. Sarkar, R. Djenadic, D. Wang, C. Hein, R. Kautenburger, O. Clemens, H. Hahn, *J. Eur. Ceram. Soc.* **2018**, *38*, 2318–2327.
[22] J.-W. Yeh, S.-J. Lin, *J. Mater. Res.* **2018**, *33*, 3129–3137.
[23] J. Zhou, J. Zhang, F. Zhang, B. Niu, L. Lei, W. Wang, *Ceram. Int.* **2018**, *44*, 22014–22018.
[24] T. Jin, X. Sang, R. R. Unocic, R. T. Kinch, X. Liu, J. Hu, H. Liu, S. Dai, *Adv. Mater.* **2018**, *30*, 1707512.
[25] R. Z. Zhang, F. Gucci, H. Zhu, K. Chen, M. J. Reece, *Inorg. Chem.* **2018**, *57*, 13027–13033.
[26] D. Bérardan, S. Franger, A. K. Meena, N. Dragoe, *J. Mater. Chem. A* **2016**, *4*, 9536–9541.
[27] D. B. Miracle, O. N. Senkov, *Acta Mater.* **2017**, *122*, 448–511.
[28] N. Qiu, H. Chen, Z. Yang, S. Sun, Y. Wang, Y. Cui, *J. Alloys Compd.* **2019**, *777*, 767–774.
[29] B. B. Berkes, A. Jozwiuk, M. Vračar, H. Sommer, T. Brezesinski, J. Janek, *Anal. Chem.* **2015**, *87*, 5878–5883.
[30] A. Schiele, T. Hatsukade, B. B. Berkes, P. Hartmann, T. Brezesinski, J. Janek, *Anal. Chem.* **2017**, *89*, 8122–8128.
[31] C. C. Nguyen, B. L. Lucht, *J. Electrochem. Soc.* **2014**, *161*, A1933–A1938.
[32] C. Xu, F. Lindgren, B. Philippe, M. Gorgoi, F. Björefors, K. Edström, T. Gustafsson, *Chem. Mater.* **2015**, *27*, 2591–2599.
[33] B. Breitung, P. Baumann, H. Sommer, J. Janek, T. Brezesinski, *Nanoscale* **2016**, *8*, 14048–14056.
[34] A. Schiele, B. Breitung, T. Hatsukade, B. B. Berkes, P. Hartmann, J. Janek, T. Brezesinski, *ACS Energy Lett.* **2017**, *2*, 2228–2233.
[35] P. Novák, F. Joho, R. Imhof, J.-C. Panitz, O. Haas, *J. Power Sources* **1999**, *81–82*, 212–216.
[36] B. B. Berkes, A. Schiele, H. Sommer, T. Brezesinski, J. Janek, *J. Solid State Electrochem.* **2016**, *20*, 2961–2967.
[37] S.-K. Jung, H. Gwon, J. Hong, K.-Y. Park, D.-H. Seo, H. Kim, J. Hyun, W. Yang, K. Kang, *Adv. Energy Mater.* **2014**, *4*, 1300787.
[38] F. Schipper, E. M. Erickson, C. Erk, J.-Y. Shin, F. F. Chesneau, D. Aurbach, *J. Electrochem. Soc.* **2017**, *164*, A6220–A6228.
[39] L. de Biasi, B. Schwarz, T. Brezesinski, P. Hartmann, J. Janek, H. Ehrenberg, *Adv. Mater.* **2019**, *31*, 1900985.
[40] F. Lin, I. M. Markus, D. Nordlund, T.-C. Weng, M. D. Asta, H. L. Xin, M. M. Doeff, *Nat. Commun.* **2014**, *5*, 3529.
[41] M. Metzger, B. Strehle, S. Solchenbach, H. A. Gasteiger, *J. Electrochem. Soc.* **2016**, *163*, A798–A809.
[42] A. T. S. Freiberg, M. K. Roos, J. Wandt, R. de Vivie-Riedle, H. A. Gasteiger, *J. Phys. Chem. A* **2018**, *122*, 8828–8839.
[43] C. L. Campion, W. Li, B. L. Lucht, *J. Electrochem. Soc.* **2005**, *152*, A2327.
[44] Y. Koyama, T. Mizoguchi, H. Ikeno, I. Tanaka, *J. Phys. Chem. B* **2005**, *109*, 10749–10755.
[45] B. Xu, C. R. Fell, M. Chi, Y. S. Meng, *Energy Environ. Sci.* **2011**, *4*, 2223–2233.

Manuscript received: January 15, 2020
Accepted manuscript online: January 16, 2020
Version of record online: ■■, ■■■

ARTICLES

Which gas will it be? Multicomponent oxides and oxyfluorides are promising electrode materials for battery applications because of their robust performance enabled by entropy stabilization. This work provides insight into adverse side reactions on both cathode, $Li(Co_{0.2}Cu_{0.2}Mg_{0.2}Ni_{0.2}Zn_{0.2})OF$, and anode, $(Co_{0.2}Cu_{0.2}Mg_{0.2}Ni_{0.2}Zn_{0.2})O$, leading to gas evolution in Li-ion cells during cycling operation.